POLITECNICO DI TORINO
Repository ISTITUZIONALE

Collapse analysis of the Polcevera viaduct by the applied element method

Original
Collapse analysis of the Polcevera viaduct by the applied element method / Domaneschi, M., Pellecchia, C., De Iuliis, E., Cimellaro, G.P., Morgese, M., Khalil, A.A., Ansari, F.. - In: ENGINEERING STRUCTURES. - ISSN 0141-0296. - STAMPA. - 214:(2020), pp. 1-11. [10.1016/j.engstruct.2020.110659]

Availability:
This version is available at: 11583/2818067 since: 2020-04-29T18:57:21Z

Publisher:
Elsevier Ltd

Published
DOI:10.1016/j.engstruct.2020.110659

Terms of use:

This article is made available under terms and conditions as specified in the corresponding bibliographic description in the repository

Publisher copyright
Elsevier postprint/Author's Accepted Manuscript

© 2020. This manuscript version is made available under the CC-BY-NC-ND 4.0 license
http://creativecommons.org/licenses/by-nc-nd/4.0/.The final authenticated version is available online at:
http://dx.doi.org/10.1016/j.engstruct.2020.110659

(Article begins on next page)

01 November 2026

Engineering Structures 000 (2019) 000000

Contents lists available at ScienceDirect

Engineering Structures

journal homepage: www.elsevier.com/locate/engstruct

Collapse analysis of the Polcevera Viaduct by the Applied Element Method

M. Domaneschi [a*], C. Pellecchia [b], E. De Iuliis [b], G. P. Cimellaro [a], M. Morgese [d], A.A. Khalil [c], F. Ansari [d]

[a] Dept. of Structural, Geotechnical and Building Engineering, Politecnico di Torino, Italy,
[b] Applied Science International Europe, Kennedy 98 St., 86170, Isernia, IS, Italy
[c] Applied Science International, LLC, 2012 TW Alexander Dr., P.O. Box 13887, Durham, NC
[d] Dept. of Civil and Material Engineering, University of Illinois at Chicago, USA

ARTICLE INFO

Keywords:
Numerical Simulations
Applied Element Method
Collapse
Bridge

ABSTRACT

On August fourteen of 2018, a portion of the highway connection viaduct over the Polcevera Valley in Genoa, Italy collapsed, and resulted in forty-three deaths, and many injuries. In the aftermath of the tragic event, in search of answers, a number of studies focused on various scenarios pertaining to the causes of the collapse, i.e. sustained effects of fatigue and corrosion, lack of redundancy, construction abnormalities, and others. In the study reported herein, post collapse analysis of the Morandi's Polcevera viaduct was conducted by the applied element method (AEM). AEM made it possible for step-by-step evaluation of the structural response of the bridge model to progressive reduction of the strength capacity of single macro-components. In using the proposed approach, it was not necessary to consider the factors that may have resulted in the capacity degradation of the structural elements, such as fatigue and corrosion. Instead, structural degradations were introduced in the model as an incremental area reduction factor until complete section loss was reached. The results of the analyses revealed that the stay cable was the most critical element whose failure would have triggered the collapse. The simulation model further indicated that if sections other than the stay cable had triggered the collapse, such as the main girder, the large visible displacements involved in their collapse, would have warned the authorities of the impending failure. The reproduced mechanism of collapse was further validated with references to the real debris distribution observed from images and a comparison with the available video footage of the bridge collapse, released by the Italian Authorities.

® 2013 Elsevier Ltd. All rights reserved.

1. Introduction

The viaduct over the Polcevera Valley in Genoa, Italy, was built in the years between 1963 and 1967. It was about 1100 m long and 18 m wide, supported by twelve piers between two bents, Piers #1 and #12 at the extremities (Fig. 1). To overcome the Polcevera River and two sets of Railway lines, three *balanced systems* were built (Fig. 2). They consisted of A-shaped towers connected to the extremities of the main girder by prestressed concrete stays. The A-shaped towers were 90 m tall, and the deck height above the river was around 45 m. The daily traffic count over the 4-lane bridge ranged from $2x10^4$ at the inception to $1.5x10^5$ during the last years of the service life of the bridge [1-3].

The bridge Pier #9 failed on August 14, 2018 and a 250 m portion of the deck collapsed into the river and the railway lines beneath. The only major traffic on the bridge at the time of collapse pertained to that of a 44 tons truck passing by Pier #9 [4]. The collapse caused forty three deaths, and nine injuries including the motorists, and the workers of the municipal waste company below the bridge. Moreover, six hundred people were displaced from their homes near the viaduct.

Several issues concerning the various structural components of the bridge were included in a number of official reports a month following the collapse of the viaduct [5]. However, earlier visual inspections of the stays in piers number 9 and 11 during the period 1991-1992 had already highlighted that "most of the ducts did not have grouts, that supposed to have been injected in during the construction, and strands showed extensive corrosion and some cables had loose strands". For pier number 11, inspections of stays at the top of the A-shaped tower indicated that the "strands were extremely deteriorated with very strong corrosions, many elements were broken with missing injected grouts" [5]. Subsequent visual inspections in 2015 confirmed further deterioration of the stays. In addition, the dynamic tests of the balanced systems in 2017 indicated "lack of symmetric response in the mode shapes" [5]. Maintenance of degraded structural elements was planned in 2017. In particular, the maintenance program included retrofitting of the stays in Piers #9 and #10, in a similar fashion to the previous retrofits in Pier 11, where new external cables were added to provide the necessary support. Unfortunately, the bridge collapsed prior to retrofitting Piers #9 and #10 [5].

*Corresponding author. Tel.: +39 340 810 8793
E-mail address: marco.domaneschi@polito.it (M. Domaneschi).

https://
Received; in revised form; Accepted
/ © 2019 Published by Elsevier Ltd.

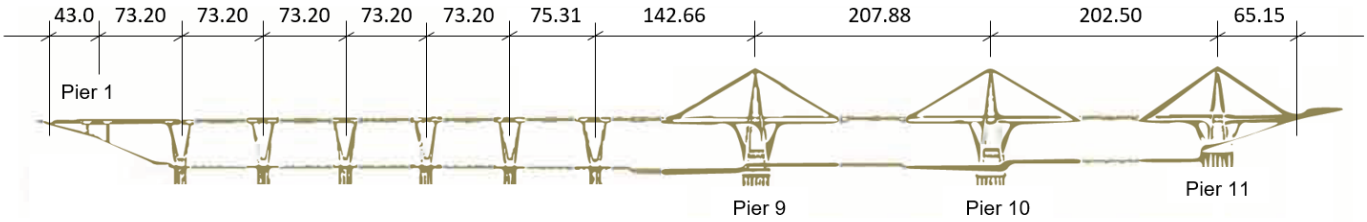


Fig. 1 – The Polcevera Viaduct [m] (*L'Industria Italiana del Cemento*, 1967) [2]

Calvi et al. [6] first discussed potential reasons for the collapse of the balanced system, prior to the availability of the collapse video footage. They also pointed at some other inadequacies of the bridge. Subsequently, Bazzucchi et al. [7] reported a description of recent failures for five bridges in Italy including the Polcevera viaduct. The report indicated that lack of information about the structural condition of the bridges was the cause for their failures.

In contrast to the previous contributions from literature, the objective of the study reported herein was to consider the role of each degraded member of the balanced system in the analysis, e.g. deck beams and the stays, in causing the collapse of the bridge. Therefore, a numerical model of the balanced system of Pier #9 was built in order to simulate the strength degradation of different structural elements and their respective contributions to the progressive collapse by way of an iterative analysis approach. Validation of the proposed approach was accomplished by references to the collapsed bridge debris distribution observed from the images and the video footage of the bridge collapse, released by the Italian Police and Fire Brigade Corps (Guardia di Finanza, 2019; Vigili del Fuoco, 2019) [8,9].

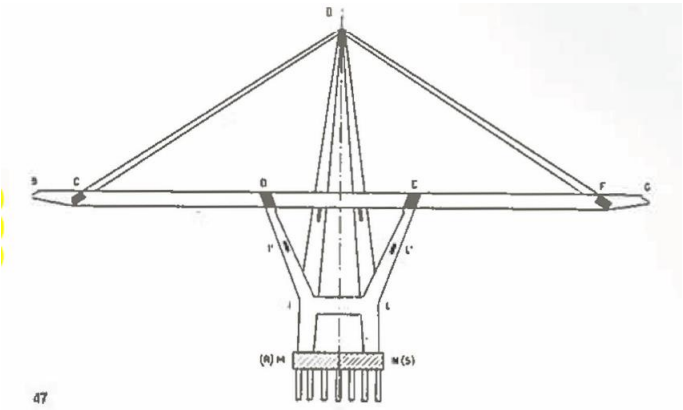


Fig. 2 – The balanced system (*L'Industria Italiana del Cemento*, 1967) [2]

The applied element method (AEM) was employed for the analysis of the collapse for this bridge. While a detailed description of AEM is beyond the scope of the present study, an abridged description of the method will be provided next for completeness. Subsequently, a description of the Polcevera Viaduct and the balanced system is provided along with its modelling. The final steps of the present study consist of (i) identification of the structural components whose strength degradation triggered the collapse of Pier #9, and (ii) comparison of the identified failure mechanism with the available media contents (images, videos, etc.). The concluding remarks complement this study with a comparative discussion with respect to some recent works on the same case study.

2. The Applied Element Method

Review of the technical literature reveals that traditional methods of structural analysis are mainly based on traditional finite element techniques that assume full compatibility at the nodes that connect the structural elements. These standard methods are computationally expensive and time demanding when full collapse analyses with prediction of debris distribution are considered (Grunwald et al., 2018) [10]. More details about the benefits of using AEM for collapse and demolition analysis of structures can be found in Grunwald et al. (2018) and Khalil (2012) [10,11].

AEM corresponds to the category of discrete element methods (DEM), and can be used for simulating the response of continuum elements [12-15]. Malomo, et al. [16] provides a comprehensive review, and describes the differences between AEM and other discrete element methods. In essence, AEM provides a new approach with capability for predicting the collapse mechanism of structures, approximately as a continuum, and accurately in discrete forms. AEM has been widely employed in the reproduction of collapse mechanisms in a variety of structural systems: e.g. in steel structures [11], failure of bridges subjected to natural hazards [6,17,18], and dynamic response up to collapse of masonry buildings [16].

AEM can track the structural collapse behavior passing through the elastic stage, the crack initiation and propagation, the reinforcement steel yielding, the element separation and the element collision (contact). Within AEM, the structure is modeled as an assembly of 8-points hexahedral elements. Therefore, each element is assumed rigid (6 degrees-of-freedom) and has a 3-D physical solid shape. Two adjacent elements are assumed to be connected by one normal and two shear springs distributed around the elements' edges on the interface. Each group of springs represents the entire stresses and deformations of a certain volume.

Fully nonlinear path-dependent constitutive models for reinforced concrete are adopted in the AEM. For concrete compression states, the elasto-plastic and fracture model by Maekawa and Okamura (1983) has been used [19]. Linear stress-strain relationship is adopted for concrete subjected to tension until the material cracks. The Menegotto and Pinto (1973) [20] constitutive relationship is employed for modeling the behavior of reinforcing bars and prestressing strands. Concrete is assumed cracked when the principal tensile stresses reaches the cracking strength of concrete.

More details on the theoretical aspects related to AEM and its comparison with finite element method can be found in (Meguro and Tagel-Din, 2000, 2001, 2002; Tagel-Din and Rahman, 2004; Grunwald et al., 2018) [21-24,10]. The AEM code *Extreme Loading for Structures* has been used to perform the collapse simulations of the balanced system [25].

The same code [25] has been also used in a pioneering study on the collapse of Pier #9 [6]. In that work, stays were modelled as nonlinear links consisting of special nonlinear springs with capability to connect the centroids of two separate solid elements, carrying axial stresses only. The AEM model consisted of 320000 degrees of freedom [25].

In the present research, stays' strands were modelled as nonlinear springs in their actual positions on the cross section of the stays' within the encased concrete, connecting face-by-face adjacent solid concrete elements. The whole model consists of 900000 degrees of freedom. Additional details pertaining to the AEM model employed herein, is provided in the ensuing section of this article.

3. The balanced system: characteristics and modelling

Polcevera Viaduct, also known as Morandi Bridge, was designed by Riccardo Morandi, and constructed between 1963 and 1967 with extensive use of reinforced concrete and the pioneering use of prestressed concrete (Morandi, 1967; 1968) [2,3]. In particular, the stays' cover was built in prestressed concrete as the box girder main deck. Fig. 3 shows the AEM numerical model of the balanced system with the Gerber connections at the extremities [25]. With respect to the balanced system employed in [6], as discussed earlier, strands were modelled as an assembly of springs in their actual positions on the cross section of the stays' concrete casing. This

provided full bonding between the strands and the stays' concrete elements. The strands continuously running over the saddle at the top of the A-shaped tower were modelled as springs. Thus, their actual curved shape was reproduced.

According to the designer [2,3], maximum compressive strengths of 37, and 50 MPa were assumed for ordinary and prestressed concrete, respectively. Yield stresses of 265, and 431 MPa were considered for corrugated steel bars in ordinary and prestressed concrete elements, respectively. High strength steel with yield strength of 1667 MPa was assumed for strands. Time dependent phenomena were not considered in the AEM model. Table 1 summarizes the materials properties values adopted in the bridge model, where E is the Young modulus, σ_c the compressive strength of concrete, σ_y the yielding stress.

In the following, a description of the adopted model with respect to the original design tables of the balanced system is provided. It consists of: (i) a reinforced concrete trestle composed by four H-shaped frames connected by cross girders (Fig. 4); (ii) An A-shaped tower, completely independent from the trestle, made up of four inclined columns with variable hollow sections (Fig. 5 and Fig. 6); and (iii) A continuous box girder of prestressed concrete with six longitudinal ribs. Prestressed cables were placed in the ribs at the intersection between the transverse beams and the trestle (e.g. Fig. 7). Additional prestressing cables were placed at the bottom of the deck.

Table 1 – Material properties

	Concrete		*Corrugated bars*		*Strands*	
	σ_c *[MPa]*	*E [GPa]*	σ_y *[MPa]*	*E [GPa]*	σ_y *[MPa]*	*E [GPa]*
Ordinary	37	35	265	210	1667	210
Pre-stressed	50	40	431	210		

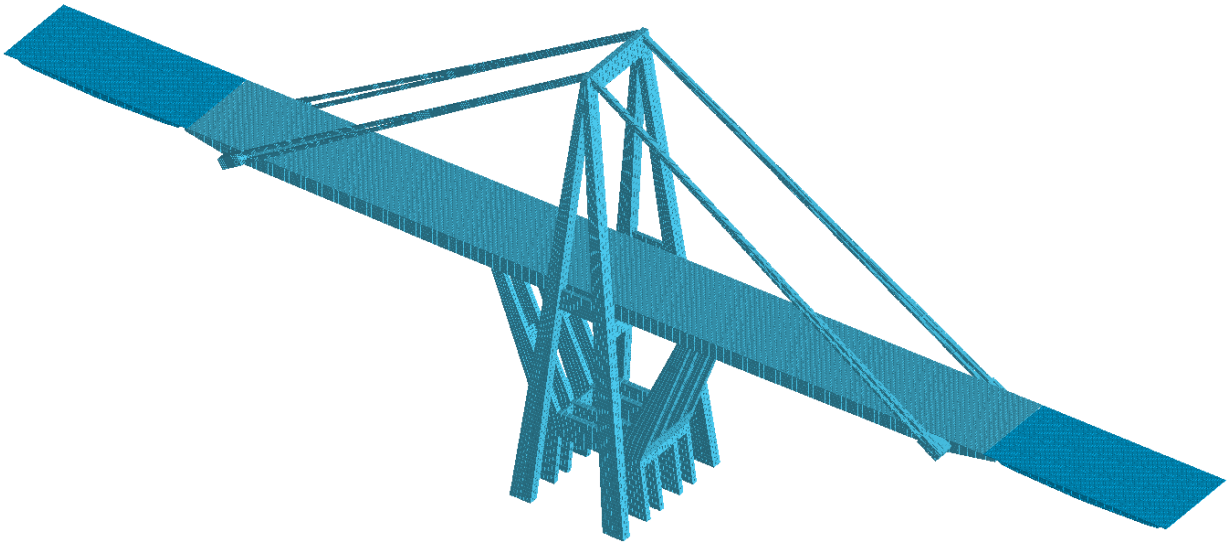


Fig. 3 – Image of the AEM model of the balanced system

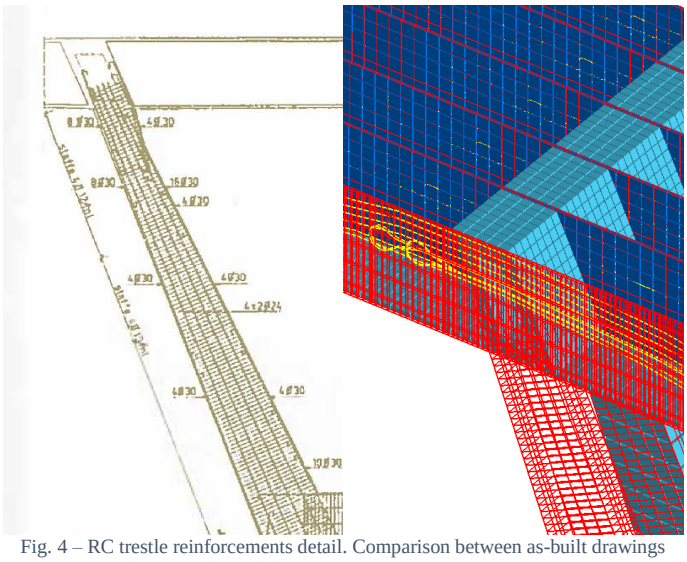


Fig. 4 – RC trestle reinforcements detail. Comparison between as-built drawings (*L'Industria Italiana del Cemento*, 1967) [2] and the AEM model

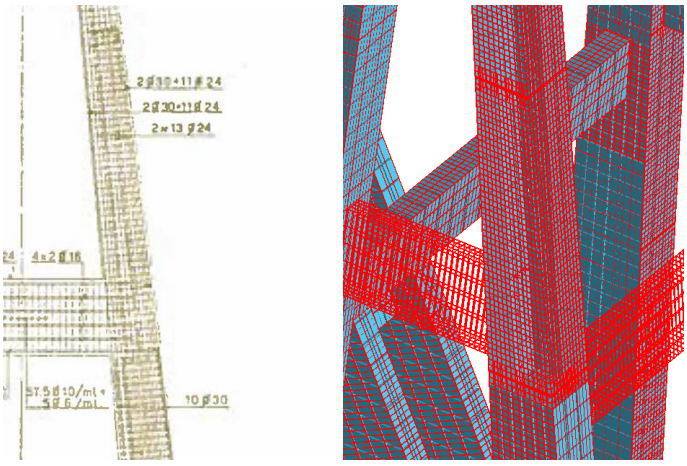


Fig. 5 – RC A-shaped tower reinforcements detail. Comparison between as-built drawings (*L'Industria Italiana del Cemento*, 1967) [2] and the AEM model

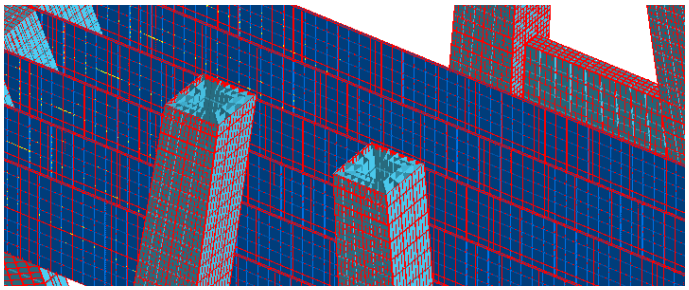


Fig. 6 – Hollow sections of tower's RC columns

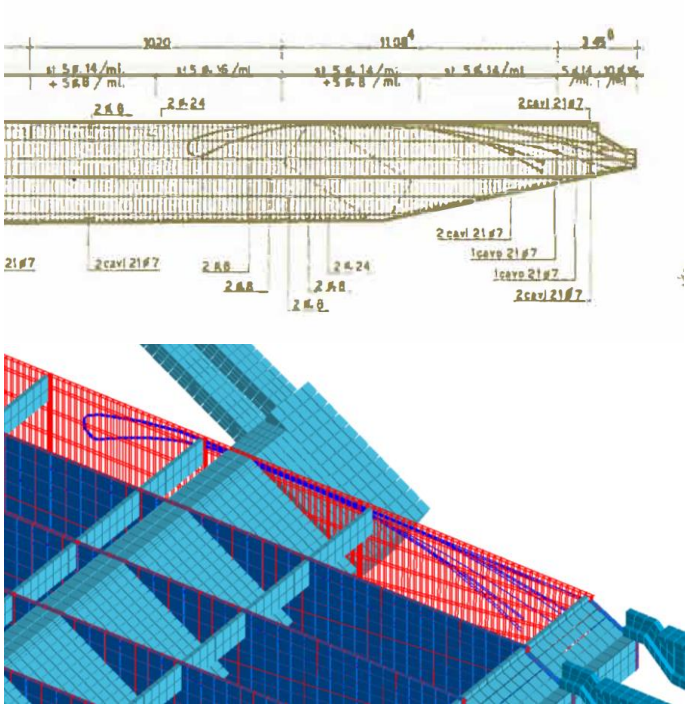


Fig. 7 – Deck's detail: prestressed cables at the connection with the stays. Comparison between as-built drawings (*L'Industria Italiana del Cemento*, 1967) [2] and the AEM model

The main girder works as a continuous beam on four supports. The trestle provides the first supports on the central portion of the system, while stay-cables passing over the top of the A-shaped tower provide additional supports at both extremities.

Different construction phases were considered by the designer (Morandi, 1967; 1968; Orgnoni et al. 2019) [2,3,26]. However, they were not fully reproduced in the adopted modelling. The modelling involved simplifications, which are described later in this section. The actual construction phases can be summarized as follows:

1. Trestle and A-shaped tower construction by employing the traditional methods in reinforced concrete.
2. Segmental cantilever construction process of the deck from the A-shaped tower. Each new segment was supported by temporary almost horizontal cables.
3. Installation of primary Cables A, from the A-shaped tower to the deck extremities for supporting the dead loads, and removal of temporary cables employed in phase 2.
4. Construction of the simply supported (Gerber) spans.
5. Preparation of the form-works for construction of concrete elements surrounding Cables A to be post-tensioned by the embedded secondary Cables B. Such prestressed concrete elements were intended to encase and protect steel Cables A and B. During this phase, integration of the cables in the system was accomplished by injection of grouts in the ducts.

The stays had variable cross-sections: at the deck connection they were split in two 98x61 cm rectangles to spread the effect of the concentrated force. At the top of the A-shaped tower around the saddle, the cable was composed of a single 98x122 cm rectangle (Fig. 8). The cross-sectional area and the number of strands within each cross section remained the same.

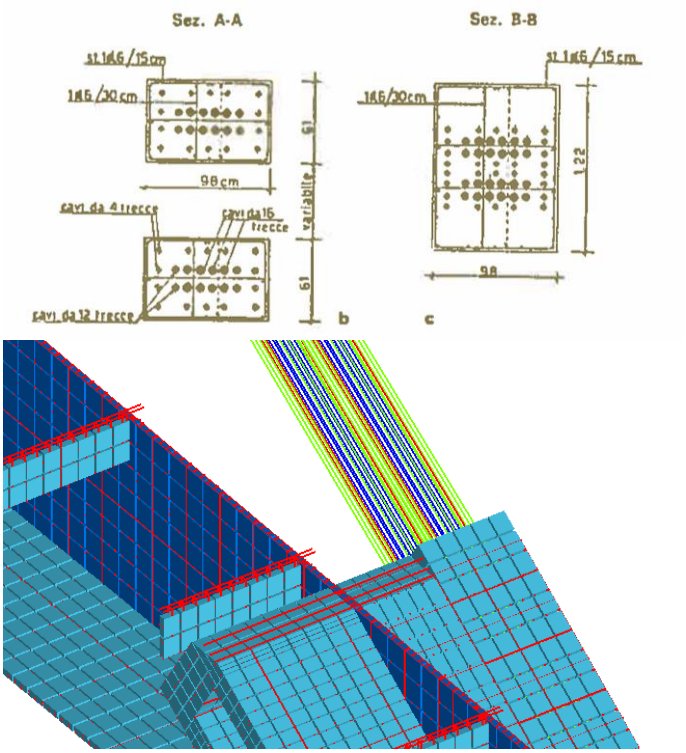


Fig. 8 – Stay-cables: primary (blue and red) and secondary (green) tendons in the AEM model. Comparison with as-built drawings (*L'Industria Italiana del Cemento*, 1967) [2] and the AEM model

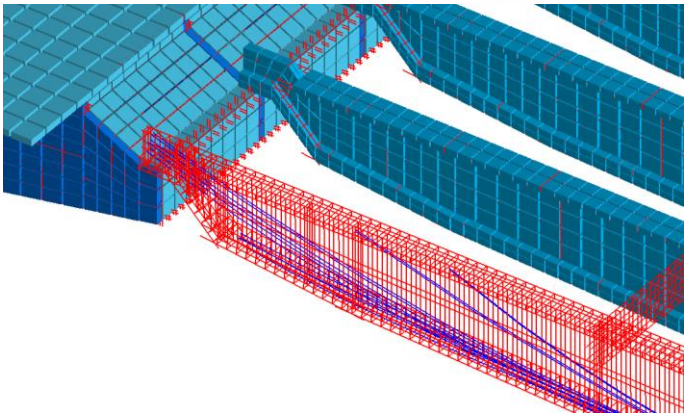


Fig. 9 – Gerber girders. Comparison between as-built drawings (*L'Industria Italiana del Cemento*, 1967) [2] and the AEM model

Cables A, the inner cables, were the first to be installed and were composed of 8 units of 12 strands each, and 16 units of 16 strands each (352 total

strands). Cables B were composed of 28 units of 4 strands each (112 total strands). All the strands had half inch (1/2") diameters.
In the design, the steel cables were encased within the prestressed concrete, mainly for the purpose of reducing the difference between the stiffnesses of the stays and the deck, and to protect the stays against corrosion. Furthermore, injection of the grout in the ducts containing steel tendons were originally planned to monotonize the entire composite structural element.
Gerber beams were installed to connect the adjacent piers (Fig. 9). A bearing materials was employed at the interface between the box girder and the Gerber beams in order to allow sliding along the horizontal axes [17].
Sensitivity analyses identified the suitable mesh size and analysis time step parameters. In doing so, both parameters were decreased during the analysis until convergence in the deck's displacement and cable's catenary shape were reached. Then, a collapses scenario was assumed to determine a suitable time step for collapse behavior. Analysis with time step higher than 0.001 showed unrealistic collapse behavior. Finally, 0.001 s time step and approximately 150000 solid elements were employed for the analyses. This led to a total computation time of almost 48 hours. Each solid element had 8 nodes, 6 degrees-of-freedom (3 translations and 3 rotations), and five springs per elemental face. A 6 core 3.50 GHz processor with 64Gb RAM and SSD drive was employed in the aforementioned computations.
The bridge model was considered fixed at the base, thus no soil-structure interaction was considered in the analysis. The construction sequence in the analysis refers to a simplified scheme with the aim of collapse reproduction. It consists in the application of the post-tensioning forces in the stays' strands, and then in the generation of the simply supported Gerber beams. The other structural components, such as the main deck, were generated at the early stages of the analysis. Vertical loads were applied as lumped masses.
The post-tensioning forces in the stays were calibrated to match the design stresses reported by the designer [2,3]. Accordingly, the tensile stresses in the stays' strands ranged between 675 to 735 MPa. In this simplified approach, attention was given to the strands because their strength degradation would be detrimental to the bridge. The simplification pertained to assuming rigid interface between the strands and the concrete. Because of this simplification there was approximately 25 MPa higher compressive stresses in the concrete surrounding the stays with respect to the actual stresses of around 5 MPa. However, this simplification was considered compatible with the aims of this study, which intended to focus on the overall behavior of the system rather than on local phenomena, such as concrete cover decompression of the bridge stays. The simplified modelling strategy introduced herein, leads to higher stresses, as opposed to the actual concrete stay stresses of approximately 5 MPa. However, the effects of the simplified assumptions do not impact the outcomes of the parametric collapse analyses that are the objective of this research.
Time-dependent phenomena, as well as construction defects were not considered in the analysis scheme described herein. The vertical displacements based on the above-mentioned analysis schemes are shown in Fig. 10.
An accurate reproduction of the construction stages for the balanced system can be found in Orgnoni et al. (2019) [26], where each stage was reproduced in detail through finite element approach and compared with the original design at several key points in terms of displacements and internal stresses. Furthermore, time dependent effects (i.e. creep and shrinkage), added masses (e.g. Jersey barriers installed during 90s), concrete stays' decompression, and defects (e.g. partial ducts injections) were also considered in order to assess the system's performance during its service life [26].
Damping was considered in the AEM model as internal damping (rate-independent). Internal damping is associated with the nonlinear response of the construction materials (e.g. concrete cracking, steel reinforcements unloading after yielding) and contact induced friction between the structural components. Furthermore, the proposed AEM model considers energy dissipation due to collision between elements and soil during collapse [25].

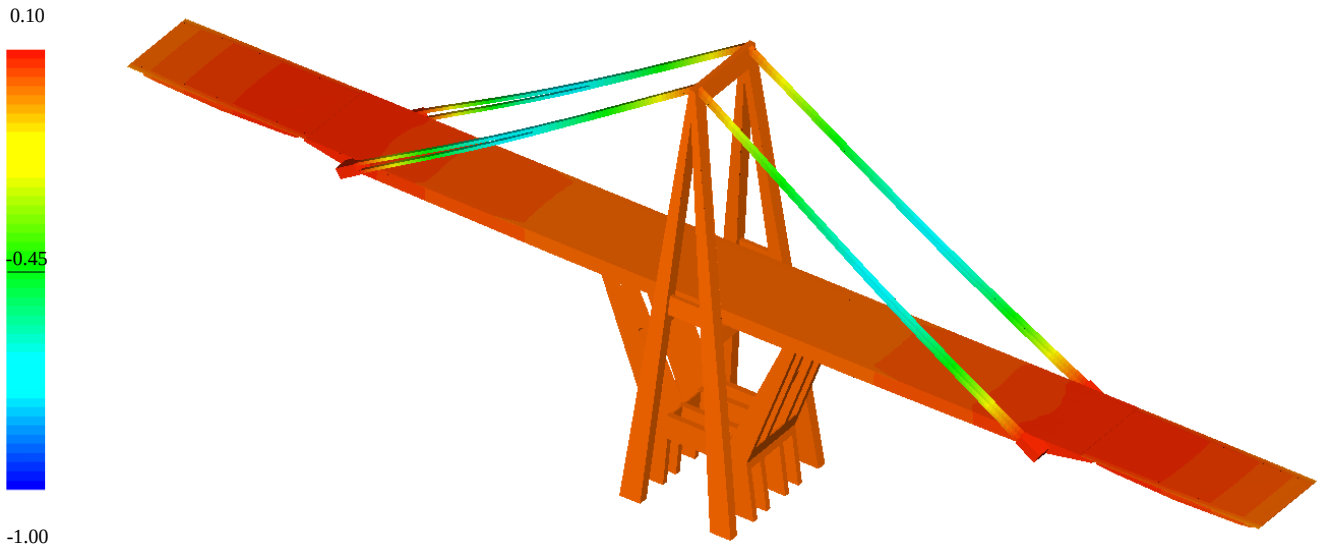
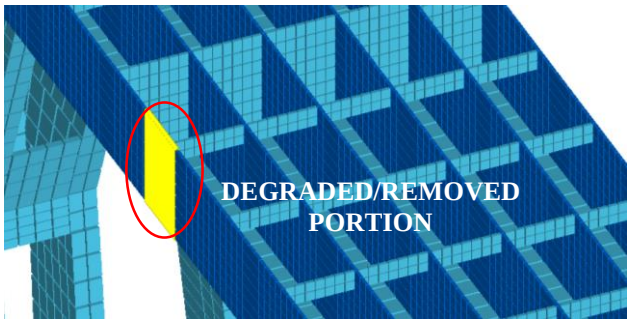
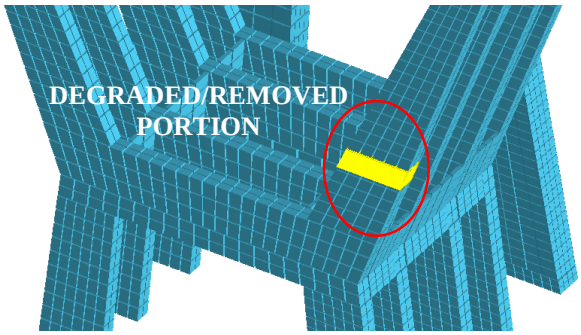
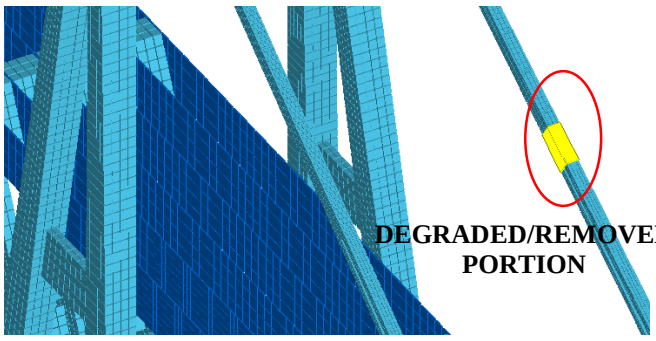


Fig. 10 – AEM model: vertical displacements due to the dead load after post-tensioning of prestressing cables [m]

Focusing on bridge loading conditions that could have contributed to the structural collapse, some considerations were done. Degradation of bridges over the duration of their service lives is usually associated with the effects of increased truck traffic [27]. Therefore, increased frequency of axle loads and amplitudes are amongst major reasons for shortening the service lives or even collapses of existing bridges [28,29].
Dynamic AEM analyses was performed by considering the response of the bridge to the dynamic effects of moving traffic, and for comparison with the response due to self-weight. The automobile induced loads were modelled by considering the effects of two axles, exerting a load equal to 2 tons to the bridge. Trucks were modelled by 5 equidistant axles, resulting in a total load of 44 tons. Both automobiles and trucks were considered travelling along the two traffic directions on the bridge.
The dynamic preliminary analyses on the developed AEM model indicated that the effects of live loads were overshadowed (2-5%) in comparison to those induced by dead loads. The same outcome can be found in Calvi et al. (2018) [6], where the findings indicated that the live loads consisted of only a small fraction of the permanent loads. Indeed, the box girder of the bridge consisted of extremely heavy reinforced and prestressed concrete elements. For instance, the weight of a 44 tons' truck was estimated less than 1% of the deck dead load, i.e. around 4500 tons considering a total length of approximately 170 m between the stays' connections, and a width of 15 m.

Therefore, traffic load did not have a considerable effect, in terms of the collapse analyses by the AEM model. However, the traffic loads played an important role in the degradation of the stays' support system of the actual structure. As shown in Orgnoni et al. (2019) [26], traffic loading generated tensile stresses in the concrete ducts of the stay cables, which in turn caused opening of the cracks that facilitated corrosion of steel reinforcements and the cables. Furthermore, as shown by the classical influence line analysis in Morgese et al. (2020) [28], other factors in combination with the truck axle loads contributed to the bridge collapse. As discussed earlier, in the present study, only the effect of self-weight is considered in the AEM collapse analyses.

Table 2 – Performed analysis during the first stage of numerical simulations

Element	Area of the local degradation/removal	Number of degraded/removed portions	Analysis results
DECK		*3 RIBS*	*No-collapse: the structure is able to redistribute the loads between the other elements*
		4 RIBS	*Collapse*
TRESTLE		*4 COLUMS*	*No-collapse: the structure is able to redistribute the loads between the other elements*
		5 COLUMNS	*Collapse*
STAY		*1 STAY*	*Collapse*

4. Parametric collapse study

This study did not concentrate on the factors that may have resulted in the capacity degradation of the structural elements. Instead, it followed a macro-structural component approach, evaluating the step-by-step structural response of the model to the progressive reduction of the strength capacity of single macro-components. Hence, the analysis of the collapse was performed through an iterative approach, assuming an increase of section loss in different elements of the balanced system. For example, the strength capacities of the deck ribs were progressively reduced until the collapse occurred. Degradations were introduced in the model as an incremental area reduction factor, till the complete section loss was reached. This was done without explicit modelling of the degradation processes, e.g. fatigue or corrosion.

Table 2 summarizes the local incremental section removal assumptions employed in this study. For the deck and the trestle, removal corresponded to the transvers section reduction of both steel reinforcements and concrete. For stays, damage corresponded to the transvers section reduction of steel reinforcements only. The proposed damage analysis approach was implemented through incremental reduction of the properties of the spring elements that connect the rigid elements of the model.

During the analyses, the incremental reduction of the steel properties was allowed up to 90% decrease in the original strength of the section. Hence, by circumventing total section loss, it was possible for the stresses to redistribute and, therefore, avoiding computational difficulties. For

example, when the rib of the main girder reached the 90% damage level without collapse, removal process would continue in the subsequent ribs until the commencement of collapse.
The first outcome of the sensitivity analysis on the progressive collapse of the bridge highlighted the robustness of the trestle and of the deck. This result was justified in view of the redundancy that characterize these structural elements and their compression state in in-service condition. Indeed, the trestle elements were predominantly in compression. Similarly, the main girder was subjected to high compressive forces because of the horizontal components of the internal forces in the stays. In essence, all the deck sections were in a prevalent compression state under the working loads.

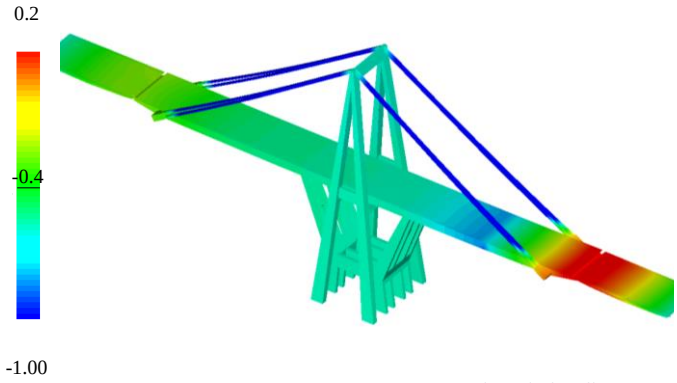


Fig. 11 – Vertical displacement with section removal at three deck's ribs [m]

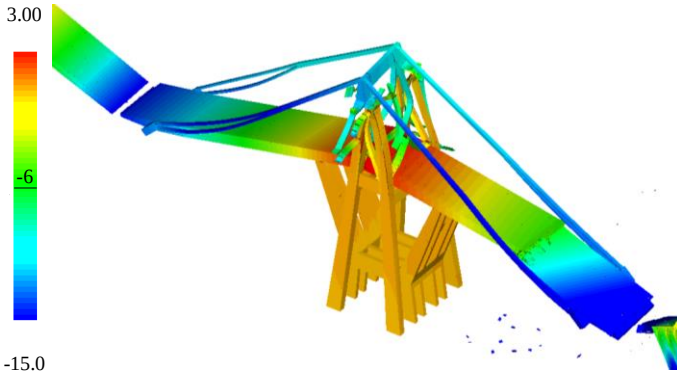


Fig. 12 – Vertical displacement with section removal at four deck's ribs [m]

On the other hand, the failure of one cable leads to the failure of the main deck due to lack of torsional capacity, and consequently, the entire structure collapses (Fig. 15).
Analysis of the incremental section loss in different elements of the structure revealed that stay cable is the most critical element whose failure triggers the collapse. If sections other than the stay cables were responsible for the collapse, large deformations and displacements would have warned the authorities of the impending failure.
To identify the most vulnerable cross section of the stays that culminated in progressive collapse, additional analyses were performed. To accomplish this goal, the incremental section removal approach was also performed along the entire length of the strands within the stays. The results shed light into the first occurrence of failure at the connection between the stay and the saddle top of the A-shaped tower (Fig. 16).

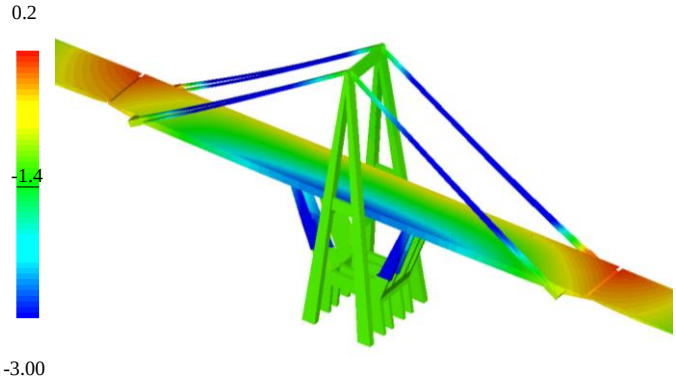


Fig. 13 – Vertical displacement with section removal at four trestle's sections [m]

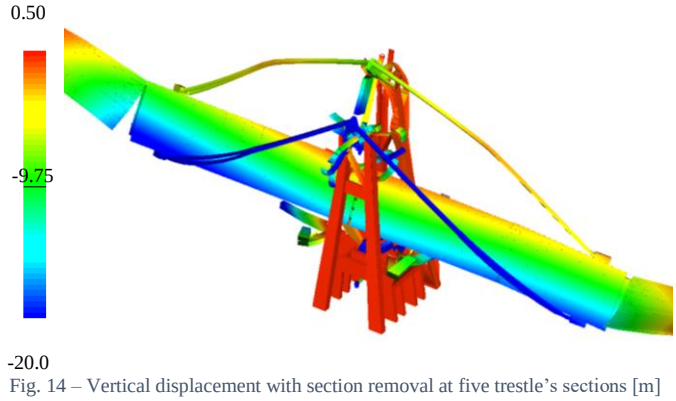


Fig. 14 – Vertical displacement with section removal at five trestle's sections [m]

The collapse of the balanced system did not occur, even following the reduction in the global capacities of three deck ribs. The bridge was still able to redistribute the loads, even when the deck deflected by about 1 m (Fig. 11). The bridge collapsed when four deck ribs reached their maximum removal limits (Fig. 12).
Similarly, even full section loss of four out of eight trestle columns did not lead to collapse of the bridge, considering the large vertical displacements as shown in Fig. 13. The collapse occurred when the fifth trestle section was fully removed (Fig. 14).

5. Modelling the release of the South-East stay

The outcomes of the analyses in the previous section of this article allowed for the identification of the component and the section that may have triggered the progressive collapse. The numerical simulations described in this section are focused on the comparison with the available documents, such as the video footage released by the authorities [9]. In particular, the failure of the South-East stay was reproduced, by gradually degrading the strands at the connection between the stay and the saddle at the top of the A-shaped tower (Fig. 17). In total around 60 % of the cross section of the strands was removed for simulating the strength degradation. The simulations were compared, frame by frame, with the images derived from the collapse footage to allow an improved interpretation of the mechanism (Fig. 18).

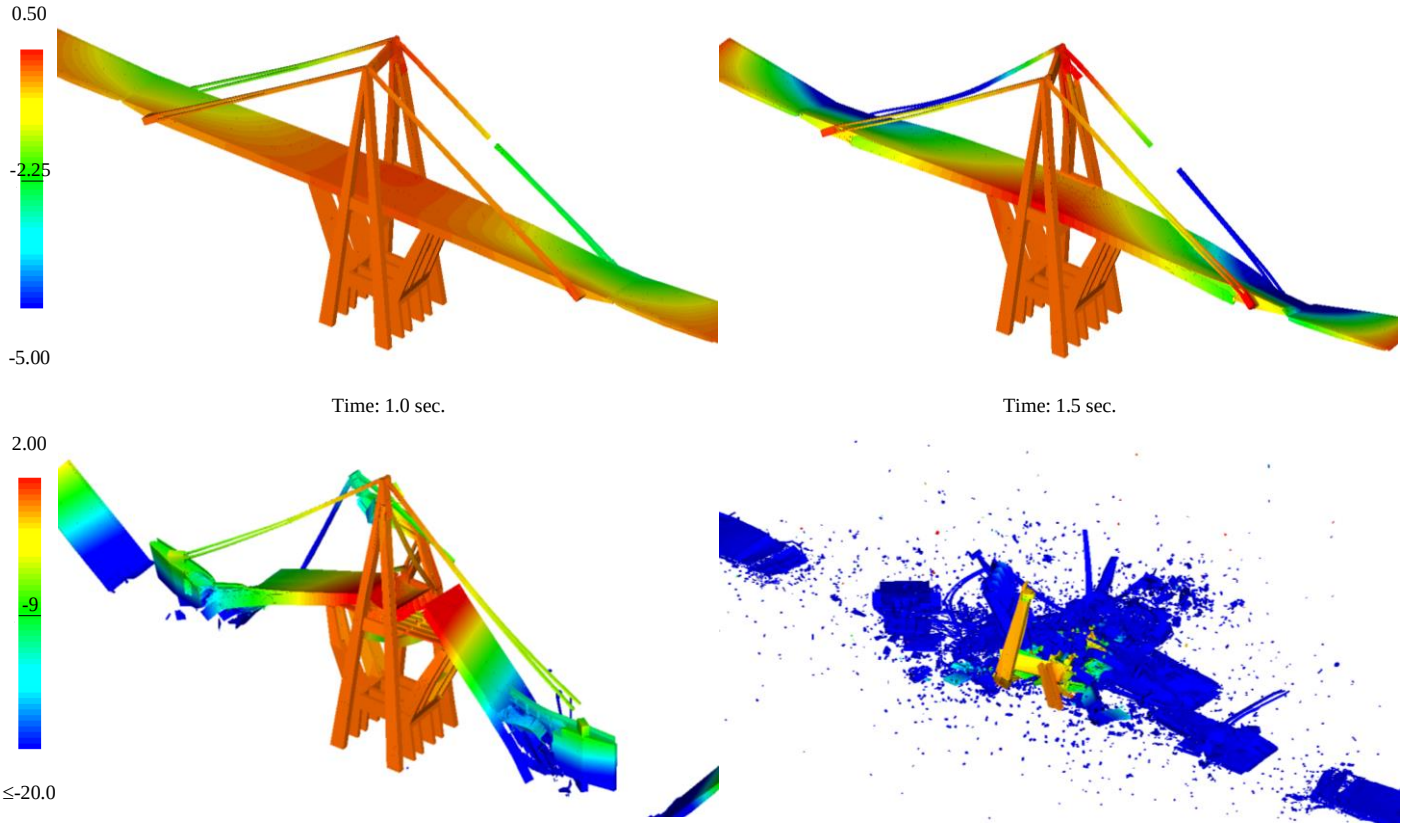


Fig. 15 – Vertical displacement with applied section removal at one cable's section [m]

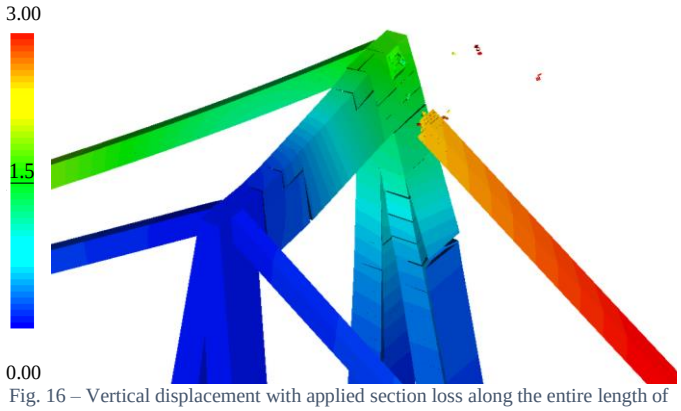


Fig. 16 – Vertical displacement with applied section loss along the entire length of the stay [m]

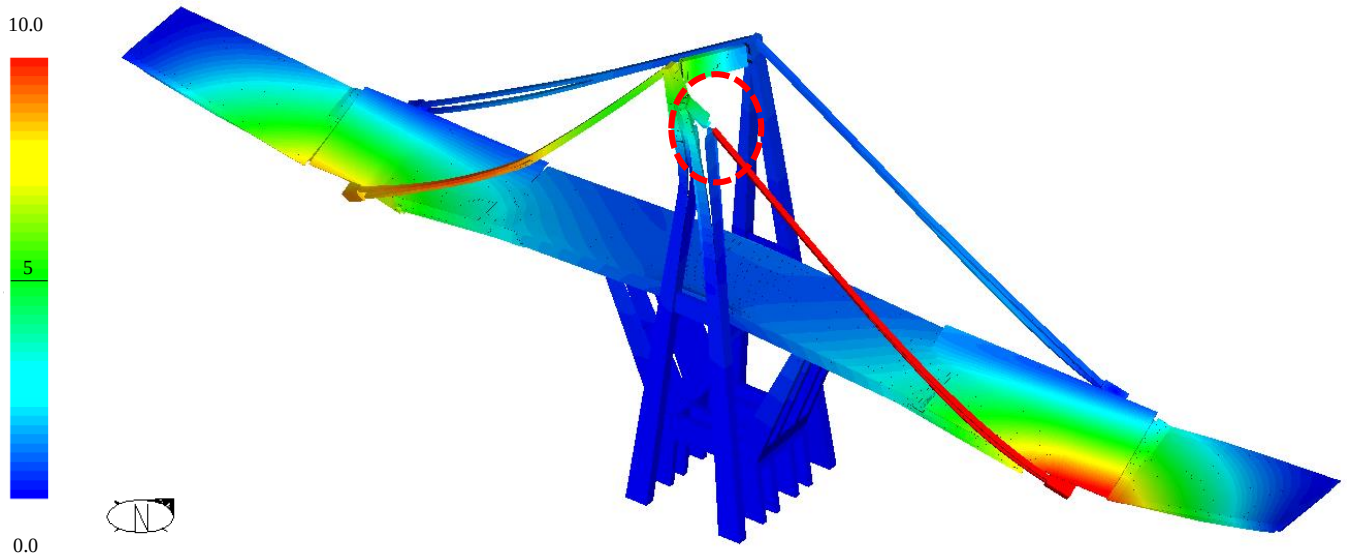


Fig. 17 – Vertical displacement with localized section loss to the South-East stay (red circle, dashed line) [m].

The first step at the 1-second time instant in Fig. shows the collapsing bridge deck that has lost its support at the South-East stay. The bridge starts to collapse, and the end of the deck at the east side undergoes relevant displacements in vertical direction. The southwest stay breaks the tower, and at the same time, the deck breaks in two points.

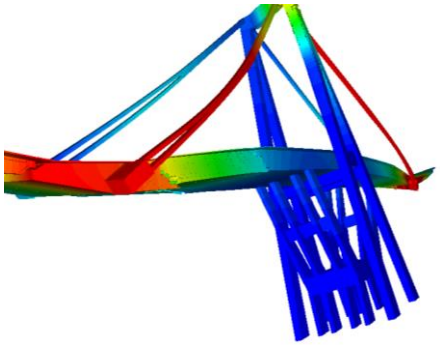
At the 2-second time instant, the deck twists around the longitudinal axis because of the pull from the standing support at the north side stay. By the 3-second time instant, the deck has already broken into a "V" shape. The south saddle at the top of the A-shaped tower has also collapsed during this time interval. It is also worth noticing that the western portion of the deck sticks vertically into the ground.

However, a discrepancy can be observed in the video footage from the 5 second time instant onwards, when the downstream (South) part of the tower is still standing up until the 9-second time instant, but in the model it collapses much earlier.

Correspondence between the computational model and the footage at the 3-second time instant can be also observed by the rotation of the western section of the deck with respect to the transvers axis of the bridge. In essence, the western section of the deck rotated during the collapse, and rested on the ground without turning itself around.

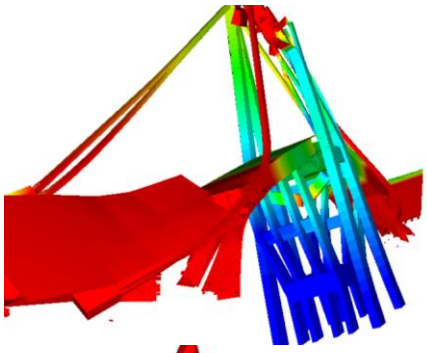
Fig. shows the post collapse shape and distribution of the debris by the computational model and the real distribution of the debris. The comparison shows satisfactory agreement between the simulated and actual debris shapes. Slight differences between the two are related to the rigid model adopted for the soil. It does not allow for the penetration of any debris into the ground. Moreover, some site details, such as the railway and the buildings were not modelled and, therefore, they can't interact with the debris distribution.

A similar parametric study was conducted by Malomo et al. (2020) [30] prior to the release of the collapse video. The results from this study, indicated the sensitivity of the collapse model, when details of the actual collapse of the balanced system are not known a priori, e.g. configuration, position of the deck, post-tensioning cables and reinforcements. This may thus justify the slight differences between the numerical results of the present study with the video footage and debris distribution.



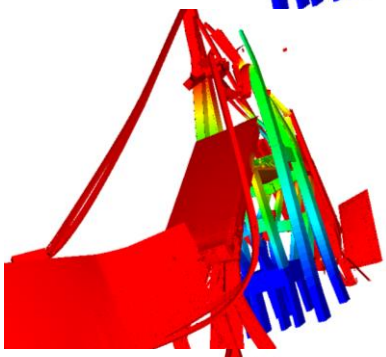


Time: 1.00 sec



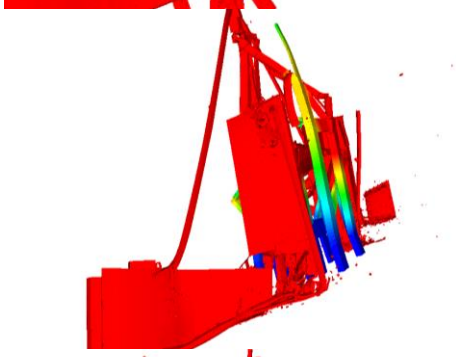


Time: 2.00 sec



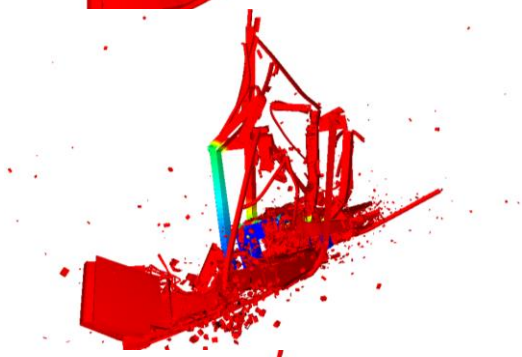


Time: 3.00 sec



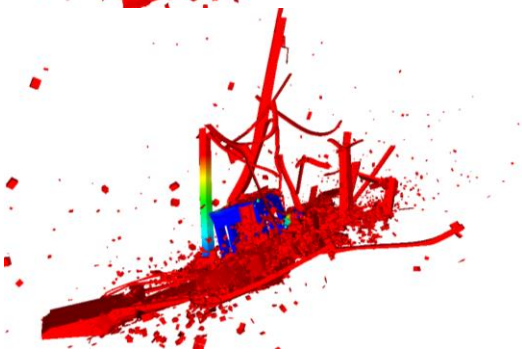


Time: 5.00 sec





Time: 6.00 sec





Time: 7.00 sec



Fig. 18 – Side by side comparison of the collapse mechanism of the bridge. Analysis results (left), actual collapse images (right) [9].

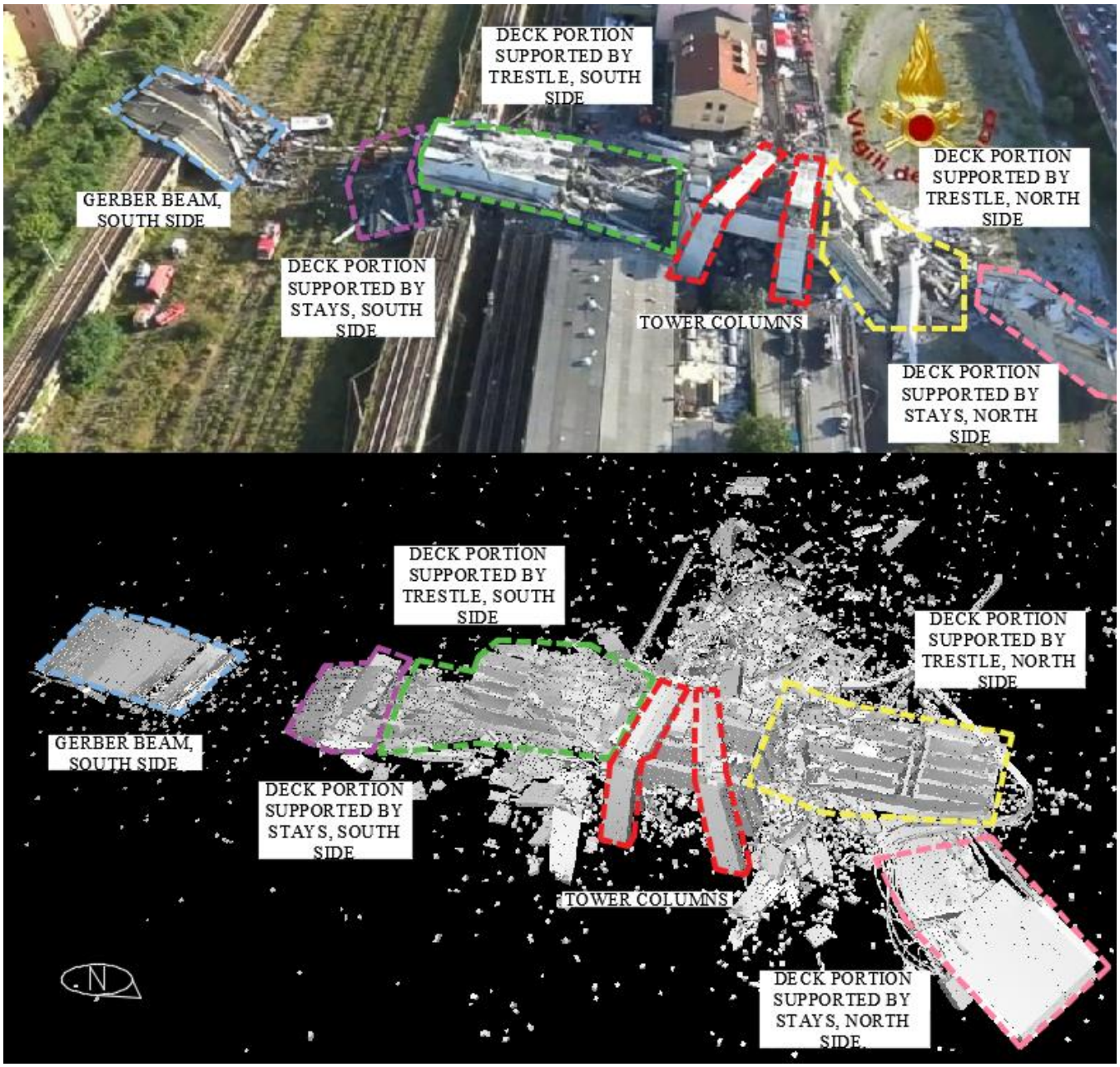


Fig. 19 – Debris heap from a picture of the Italian Fire Brigade Corps (above) [8] and same view of the collapsed shape of the AEM model (below)

6. Conclusions

In the study reported herein, post collapse analysis of the Morandi's Polcevera viaduct was conducted by AEM. A numerical model of the balanced system of Pier #9 was built, in order to simulate the strength degradation of different structural elements and their respective contributions to the progressive collapse of the bridge segments. The role of each degraded member, such as deck ribs, trestle columns and stays within the balanced system was considered in the analysis.

Validation of the proposed approach was accomplished by references to the collapsed bridge debris distribution observed from the images and the video footage of the bridge collapse, released by the Italian Police and Fire Brigade Corps. A macro-structural component approach in AEM was employed, making it possible for step-by-step evaluation of the structural response of the model to progressive reduction of the strength capacity of single macro-components. Unlike the earlier studies, the present approach did not concentrate on the factors that may have resulted in the capacity degradation of the structural elements. Instead, structural degradations were introduced in the model as an incremental area reduction factor until complete section loss was reached. This was done without explicit modelling for the actual causes of damage, such as fatigue and or corrosion.

The computational approach pertaining to the incremental damage in different sections of the structure revealed that the stay cable was the most critical element whose failure would have triggered the collapse. The simulation model further indicated that the failure of the other sections of the bridge, such as the main girder involved large displacements. Hence, if sections other than the stay cables were responsible for the collapse, large deformations and displacements would have warned the authorities of the impending failure.

Additional analysis of the stay cable by the incremental degradation approach revealed that the stay failure occurred at the connection between

the stay and the saddle top of the tower. In particular, a reasonable agreement between the actual collapse mechanism and the simulation model was achieved when the strands in the southeast stay lost 60% of its cross-section at the connection between the stay and the top of the A-shaped tower. The identified mechanism of collapse was further validated with references to the real debris distribution observed from images and a comparison with the footage of the bridge collapse, released by the Italian Authorities. However, the one-to-one correspondence between the official video footage of the collapse and the results of the analysis were fully in agreement only for the first 3-5 seconds of the collapse duration. These results are relevant considering the simplifications in modeling, and the influence of unforeseen conditions at the site of the bridge.

7. Acknowledgements

Guardia di Finanza and Vigili del Fuoco Corps are gratefully acknowledged for making images of the collapse of the infrastructure available for publication. Furthermore, the Editorial Board of the Industria Italiana del Cemento are also acknowledged for making available the original design details.
This research has received funding from the European Research Council under the Grant Agreement n° ERC_IDEAL RESCUE_637842 of the project IDEAL RESCUE—Integrated Design and Control of Sustainable Communities during Emergencies.

8. References

[1] AISCAT - Italian Association of Motorway and Tunnel Dealers, http://www.aiscat.it/pubblicazioni.htm?ck=1&nome=pubblicazioni&idl=4, Accessed October 1, 2019.

[2] Morandi R. Il viadotto sul Polcevera per l'autostrada Genova-Savona. *L'Industria Italiana del Cemento* 1967; XXXVII:849–872.

[3] Morandi R. Viaducto sobre el Polcevera, en Génova Italia. *Informes de la Construcción* 1968; 21(200).

[4] Gatti F. Ponte Morandi, le foto shock prima del crollo: travi rotte e cavi ridotti del 75 per cento. *L'Espresso* 2018 http://espresso.repubblica.it/attualita/2018/09/13/news/ponte-morandi-1.326939, Accessed June 17, 2019.

[5] Ministero delle Infrastrutture e dei Trasporti, Commissione Ispettiva Ministeriale, "Comune di Genova, Autostrada A10 – Crollo del Viadotto Polcevera, Evento Accaduto il 14 Agosto 2018", 14 Settembre 2018, Roma. Available online: http://www.mit.gov.it/comunicazione/news/ponte-crollo-ponte-morandi-commissione-ispettiva-genova/ponte-morandi-online-la, Accessed June 17, 2019.

[6] Calvi GM, Moratti M, O'Reilly GJ, Scattarreggia N, Monteiro R, Malomo D, Calvi PM, Pinho R. Once upon a Time in Italy: The Tale of the Morandi Bridge. *Structural Engineering International* 2018, 29(2):198-217.

[7] Bazzucchi F, Restuccia L, Ferro GA. Considerations over the Italian road bridge infrastructure safety after the Polcevera viaduct collapse: past errors and future perspectives. *Frattura ed Integrità Strutturale* 2018, 46:400-421. DOI: 10.3221/IGF-ESIS.46.37

[8] Vigili del Fuoco 2019, https://www.vigilfuoco.tv/, Accessed, July 16, 2019.

[9] Guardia di Finanza 2019, http://www.gdf.gov.it/, Accessed, July 16, 2019.

[10] Grunwald C, Khalil AA, Schaufelberger B, Ricciardi EM, Pellecchia C, De Iuliis E, Riedel W. Reliability of collapse simulation – Comparing Finite and Applied Element Method at different levels. *Engineering Structures* 2018; 176:265-278.

[11] Khalil AA, Enhanced Modeling of Steel Structures for Progressive Collapse Analysis Using the Applied Element Method. *Journal of Performance of Constructed Facilities* 2012, 26(6). DOI: 10.1061/(ASCE)CF.1943-5509.0000267

[12] Lemos LV, Discrete Element Modeling of Masonry Structures. *International Journal of Architectural Heritage Conservation, Analysis, and Restoration* 2007, 1(2):190-213.

[13] Cundall P A, A computer model for simulating progressive large scale movements in blocky rock systems. *Proc. Symp. Rock Fracture (ISRM)*, Nancy, 1971.

[14] Pantò B, Cannizzaro F, Caliò I, Lourenço PB, Numerical and experimental validation of a 3D macro-model for the in-plane and out-of-plane behavior of unreinforced masonry walls. *International Journal of Architectural Heritage* 2017, 11(7):946–64.

[15] Kawai T, New discrete models and their application to seismic response analysis of structures. *Nuclear Engineering and Design* 1978, 48(1):207–29

[16] Malomo D, Pinho R, Penna A. Applied Element Modelling of the Dynamic Response of a Full-Scale Clay Brick Masonry Building Specimen with Flexible Diaphragms. *International Journal of Architectural Heritage* 2019. DOI: 10.1080/15583058.2019.1616004

[17] Salem H, Mohssen S, Nishikiori Y, Hosoda A. Numerical Collapse Analysis of Tsuyagawa Bridge Damaged by Tohoku Tsunami. *Journal of Performance of Constructed Facilities* 2016, 30(6).

[18] Salem H, Mohssen S, Kosa K, Hosoda A. Collapse Analysis of Utatsu Ohashi Bridge Damaged by Tohuku Tsunami using Applied Element Method. *Journal of Advanced Concrete Technology* 2014, 12:388-402.

[19] Maekawa K, Okamura H, The Deformational Behavior and Constitutive Equation of Concrete using the Elasto-Plastic and Fracture Model. *Journal of the Faculty of Engineering* - The University of Tokyo (B) 1983, 37(2): 253-328.

[20] Menegotto M, and Pinto PE, Method of analysis for cyclically loaded reinforced concrete plane frames including changes in geometry and non-elastic behavior of elements under combined normal force and bending. *Proc., IABSE Symp. of Resistance and Ultimate Deformability of Structures Acted on by Well Defined Repeated Loads* 1973, International Association of Bridge and Structural Engineering, Libson, Portugal, 13:15-22.

[21] Meguro K, Tagel-Din H. Applied element method for structural analysis: theory and applications for linear materials. *Structural Engineering Earthquake Engineering JSCE* 2000; 17(2):215-224.

[22] Meguro K, Tagel-Din H. Applied Element Simulation of RC Structures under Cyclic Loading, *Journal of Structural Engineering ASCE* 2001; 127(11):1295-1305.

[23] Meguro K, Tagel-Din H. AEM Used for Large Displacement Structure Analysis, *Journal of Natural Disaster Science* 2002; 24(1):25-34.

[24] Tagel-Din H. and Rahman N. Extreme loading: breaks through finite element barriers. *Structural Engineer* 2004; 5(6):32–340.

[25] Applied Science International LLC. 2018. Extreme loading for structures (2018). Durham (NC), USA.

[26] Orgnoni A, Pinho R, Moratti M, Scattareggia N, Calvi GM. Revisione critica e modellazione della sequenza di costruzione del viadotto sul Polcevera (in Italian), *Digital Modelling* 2019; 25:6-32.

[27] Lu N, Noori M, Liu Y. First-passage probability of the deflection of a cable-stayed bridge under long-term site-specific traffic loading. *Advances in Mechanical Engineering* 2017; 9(1):1–10.

[28] Morgese M, Ansari F, Domaneschi M, Cimellaro GP. Post-collapse analysis of Morandi's Polcevera viaduct in Genoa Italy. *Journal of Civil Structural Health Monitoring* 2019. https://doi.org/10.1007/s13349-019-00370-7

[29] Invernizzi S, Montagnoli F, Carpinteri A. Fatigue assessment of the collapsed XXth Century cable-stayed Polcevera Bridge in Genoa, *Procedia Structural Integrity* 2019; 18:237–244.

[30] Malomo D, Scattarreggia N, Orgnoni A, Pinho R, Moratti M, Calvi GM. Numerical study on the collapse of the Morandi bridge. *Journal of Performance of Constructed Facilities ASCE* 2020; Available online at: https://doi.org/10.1061/(ASCE)CF.1943-5509.0001428